FOREX Publication
Open Access | Rapid and quality publishing

International Journal of
Electrical and Electronics Research (IJEER)
Research Article | Volume 11, Issue 3 | Pages 652-657 | e-ISSN: 2347-470X

A New Closed Loop Constant v/f Control of Induction Motor with Torque Control Based on DPWM

E. Nandhini[1*] and A. Sivaprakasam[2]
[1]*Research Scholar, College of Engineering Guindy, Anna University, Chennai, India*
[2]*Associate Professor, College of Engineering Guindy, Anna University, Chennai*

***Correspondence:** nandhini3189@yahoo.com

ABSTRACT- An easy sensor-less scalar control algorithm is described in this article as a method for controlling the speed of an induction motor. For developing a closed-loop v/f control of the induction motor drive, a torque controller with PI is implemented. The torque command was estimated by utilizing the voltage command, the feedback current, and a torque estimator. Additionally, a torque reference was provided for the Torque PI controller. Considering this, the purpose of this work is to investigate the closed-loop PI-based torque control of an induction motor drive that applies DPWM. In addition to this, it provides a description of a PI-based closed-loop torque control that works in conjunction with v/f control and tries to discover the most effective method for driving an induction motor based on an examination of Total Harmonic Distortion (THD) and torque ripple. To evaluate the performance studies of open- and closed-loop strategies with DPWM techniques for induction motor driving, the MATLAB/Simulink environment has been deployed. Experimental results have been validated.

Keywords: Discontinuous PWM, Voltage source inverter, Variable frequency drives, two level inverter, SVPWM.

ARTICLE INFORMATION
Author(s): E. Nandhini and A. Sivaprakasam;
Received: 06/03/2023; **Accepted**: 29/05/2023; **Published**: 10/07/2023;
e-ISSN: 2347-470X;
Paper Id: IJEER230213;
Citation: 10.37391/IJEER.110302
Webpage-link:
https://ijeer.forexjournal.co.in/archive/volume-11/ijeer-110302.html

Publisher's Note: FOREX Publication stays neutral with regard to Jurisdictional claims in Published maps and institutional affiliations.

1. INTRODUCTION

Several industrial applications make numerous uses of three-phase induction motors. This motor is commonly used due to its adaptability to various load conditions, simple and durable structure, and affordable acquisition and maintenance [1] – [3]. Due to the vector control system's improved dynamic response [4] – [11], numerous studies in this area have been performed. Scalar control [12] – [14], however, produces the same results with low steady-state error. Due to its widespread industrial application, the (v/f) scalar control system is therefore taken into consideration in this work. The constant V/f control technique for induction motors frequently uses proportional-integral (PI) control [15].

2. CONTINOUS (CPWM) AND DISCONTINUOUS PWM (DPWM)

In the past 20 years, several pulse width modulation (PWM) techniques have gained popularity. All those PWM are grouped as continuous PWM (CPWM) and discontinuous PWM (DPWM) [16]–[17]. Unlike DPWM, which uses a discontinuous time-varying signal, in CPWM, the modulating wave would be a continuously varying signal, which indicates that the modulation stops at some point because of the modulating waves being clamped or connected to the +ve or -ve DC bus for specific clamping durations, referred to as bus clamping PWM. The positioning of a zero (+++ or ---) vector and the division of the zero-vector duration influence both continuous and discontinuous modulation. The popular CPWM methods include space vector PWM and sinusoidal PWM. The sine wave signal is compared to a triangular carrier wave, which is of higher frequency than the reference carrier sine wave; sine triangle PWM is yet another term for sinusoidal PWM (SPWM) [18] – [20]. A significant benefit of SVPWM is that it uses the DC bus 15% more efficiently than sinusoidal PWM. Even though numerous studies [21] compare the performance of SVPWM, sinusoidal PWM, and DPWM, by comparing and evaluating the results of continuous and DPWM using experimental and simulated analysis, it is suggested that 30º DPWM outperforms all currently available DPWMs. Therefore, the focus of this article is on closed-loop torque control of an induction motor drive using 30^{o} DPWM.

3. SPACE VECTOR PULSE WIDTH MODULATION (SVPWM)

A 3-ϕ system can distinctly be described by *2-ϕ* system. As they allow for the use of the vectorial rotation attribute in a complex plane, the 2-ϕ quantities can be called as vector. The SVPWM is supposed to be a *3-ϕ* sinusoidal waveform with three axes that are 120° apart in time, yielding a space vector with a constant amplitude that revolves at a constant speed. With 2 zero vectors (+++ or ---) and 6 active vectors, the two-level inverter SVPWM method creates the V_{REF} reference voltage, that is sampled for each sub-cycle *Ts*. The switching sequence used in traditional SVPWM distributes the zero-vector duration (T_0) evenly between the two zero states *i.e.*, either +++ or --- in each sub-cycle. SVPWM can achieve a maximum control voltage of (1/ 3) VDC. *Figure 1* depicts the voltage vectors associated with

FOREX Publication
Open Access | Rapid and quality publishing
International Journal of Electrical and Electronics Research (IJEER)
Research Article | Volume 11, Issue 3 | Pages 652-657 | e-ISSN: 2347-470X

two-level inverter containing six *sectors I to VI*. As shown in *Figure 2*, the V_{REF} (reference vector) is generated by two active vectors as well as two zero vectors (+++, ---) in traditional SVPWM. For illustration, in Sector I, V_{REF} is achieved by employing V_1 and V_2 vectors for T_1 and T_2 duration, V_0 for the T_0 duration of the sub-cycle.

Here, Magnitude $V_{REF} = \sqrt{V_d^2 + V_q^2}$

Where, the two-phase quantities are,

$$V_d = \frac{2}{3}\,(V_{an} - 1/2(V_{bn} - V_{cn}))$$

$$V_q = \frac{2}{3}\,(\frac{\sqrt{3}}{2}(V_{bn} - V_{cn})$$

$$\propto = tan\sqrt{V_d/V_q}$$

$$V_{REF}T_s = V_1T_1 + V_2T_2 + V_0T_0$$

$$T_s = T_1 + T_2 + T_0$$

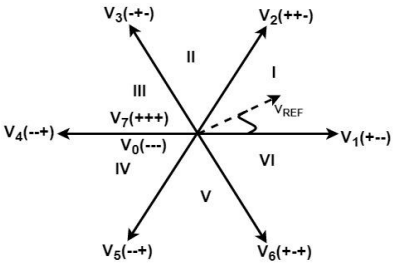

Figure 1: Switching states of SVPWM

$$T_1 = \frac{V_{REF}}{V_{DC}} \sin\frac{60-\propto}{\sin(60)} T_s \quad (1)$$

$$T_2 = \frac{V_{REF}}{V_{DC}} \sin\frac{\propto}{\sin(60)} T_s \quad (2)$$

$$\frac{T_0}{2} = \frac{1}{2}(T_s - T_1 - T_2) \quad (3)$$

4. 30° DPWM

In the conventional SVPWM each sector is divided into 60° but in 30° DPWM the 60° sector is divided into two intervals, that are fundamentally different from one another, such as it could be divided into width Υ during the first quarter cycle and (*60-*Υ) in the following quarter cycle. Since the clamping duration is split into two intervals, in the inverter states this is also termed as "Split Clamping PWM" in literature [22]-[25]. R phase is continually clamped to the *+ve* DC bus for a 30° duration as shown in *figure 2*. And it is explained for *sector I* in *figure 3*. Since one of the zero vector is removed, switching is reduced, which causes reduced switching losses as well as inverter losses along with the increase of switching frequency 1.5 times compared to SVPWM, as a result, it is frequently employed in high-frequency applications [26]-[28]. However, conduction losses are higher than those of SVPWM for high modulation indices and higher switching frequencies.

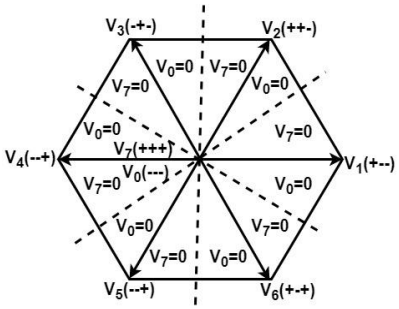

Figure 2: Voltage vectors of 30°DPWM

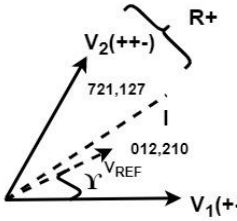

Figure 3: 30°DPWM explained for Sector I

5. A NEW CONSTANT V/F CONTROL OF INDUCTION MOTOR DRIVE

The induction motor's speed is regulated by linearly changing the voltage at the designated frequency using the v/f control approach to maintain the air-gap flux constant. The block diagram of the new v/f control of induction motor drive is shown in *figure 4*, where the torque error goes through the PI controller and generates the slip speed, which would be added to the feedback rotor speed. The voltage command is generated by a v/f function. The two main characteristics of this configuration are the inclusion of a speed tachometer, which is necessary to get the feedback rotor speed to adjust for slip frequency, and sensor-less torque estimation, which is different from the former speed-based v/f control shown in *figure 5*. The torque estimation is explained in the subsequent sections

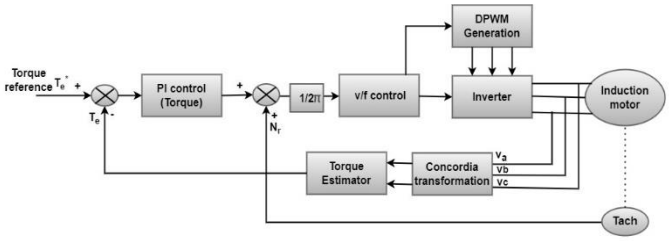

Figure 4: Block Diagram of 30°DPWM-based Closed-Loop v/f control of Induction Motor Drive with torque PI control

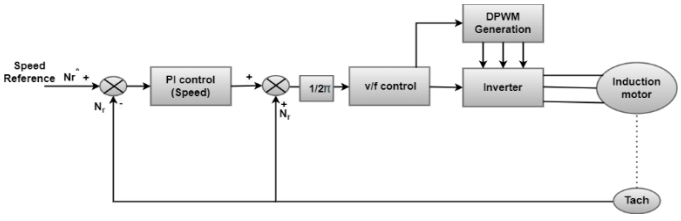

Figure 5: Block Diagram of 30°DPWM-based Closed-Loop v/f control of Induction Motor Drive with Speed PI control

FOREX Publication
Open Access | Rapid and quality publishing
International Journal of Electrical and Electronics Research (IJEER)
Research Article | Volume 11, Issue 3 | Pages 652-657 | e-ISSN: 2347-470X

5.1 Torque Estimator

The two-phase model given by the reference (α, β) [29]-[30] is the most appropriate model to examine the dynamic behavior and control algorithm design of the three-phase IM. The machine's three-phase representation (a, b, and c) is less complex with the help of this model. The following formulations provide the electromagnetic torque equations:

$$T_e = p[\widehat{\varphi_{s\alpha}}\, i_{s\beta} - \widehat{\varphi_{s\beta}}\, i_{s\alpha}]$$
$$\widehat{\varphi_{s\alpha}} = \int_0^t (v_{s\alpha} - R_s\, i_{s\alpha})dt$$
$$\widehat{\varphi_{s\beta}} = \int_0^t (v_{s\beta} - R_s\, i_{s\beta})dt$$

The transformation known as Concordia; the three-phase reference (a, b, c) can be transformed into two-phase reference (α, β) using the below transformation:

$$X_\alpha = \sqrt{\frac{2}{3}}\,[X_a - \frac{1}{2}X_b - \frac{1}{2}X_c]$$
$$X_\beta = \sqrt{\frac{2}{3}}\,[\frac{\sqrt{3}}{2}X_b - \frac{\sqrt{3}}{2}X_c]$$

With: X could be the machine's voltage, or current.

6. SIMULATION STUDIES AND RESULTS

Under varied operating circumstances, the performance of the novel constant v/f control for the IM drive based on Torque PI control has been closely reviewed. For the same 30ºDPWM, the results have been compared with Speed PI controller. *Kp = 14* and *Ki = 5* are the PI controller simulation parameters. To attain the optimal performance in terms of reduced speed overshoot and undershoot, lower settling time, and no steady-state error, the PI controller was tuned using trial-and-error method. The motor is first operated in an open loop to see what must be modified so that it can reach the target speed. The values of *Kp* and *Ki* are initially assumed to be *1* and *0*, respectively. The steady-state error has been eliminated after setting the value of *Kp*, with the optimization of rising time and overshoot, then the value of *Ki* has been increased which optimize steady-state error and settling time, then the value of *Ki* is fixed. *Table 1* lists the empirical outcomes acquired by the FFT analysis from MATLAB/Simulink for different control techniques. It demonstrates the efficacy of the suggested torque control technique since it gives lesser THD compared to prior PI speed control. The motor starts with no load for 1.5 seconds prior to getting applied with the rated load torque of 26.89N.m for 4KW induction motor are shown in *figure 6*. The simulation results are for 50Hz fundamental frequency and reference speed RPM of 1200RPM. *Figure 9 and 10* depict the stator current THD of 2.23% and voltage THD of 0.65% with their FFT waveforms for 30° DPWM based torque control, respectively. The torque smoothing waveform for torque control approach demonstrates the least torque ripple *figure 7*. The addition of torque control can improve the closed-loop *v/f* control scheme's dynamic response. The base value of the stator voltage magnitude is determined by the first PI speed using the desired V/F characteristic, and the rotor flux regulator provides the incremental voltage needed to follow the intended rotor flux without error. The second gives the slip's base value, which is calculated using the required torque and the expected rotor flux. The slip is then corrected using the torque regulator so that the desired torque is followed exactly which in turn it also reduces the THD% of current. *Figure 8* depict the torque speed waveforms for PI-based speed and torque control. The RMS (Root Mean Square) torque ripple is determined by using equation RMS torque ripple [31]-[32] and T_{av} is the average torque value.

$$T_{ripple} = \sqrt{\frac{1}{N}\sum_{1=1}^{N}(T_e(i) - T_{av})2}$$

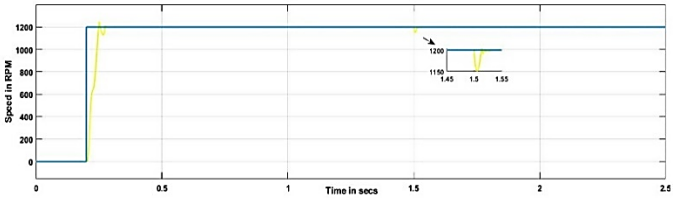

Figure 6: Reference and actual speed responses of 30° DPWM closed-loop constant v/f control with torque PI control

Table 1: Current (THD%) and Voltage (THD%) at fundamental frequency = 50 Hz and switching frequency = 10 KHz (Outcomes obtained in simulation)

Control Strategy (Constant v/f control)	Observed output voltage	Current (THD%)	Voltage (THD%)	RMS-Torque Ripple
With PI speed control based on 30 DPWM	396.3	4.65	5.72	0.007N-m
With PI torque control based on 30 DPWM	396.4	2.47	0.77	0.005N-m

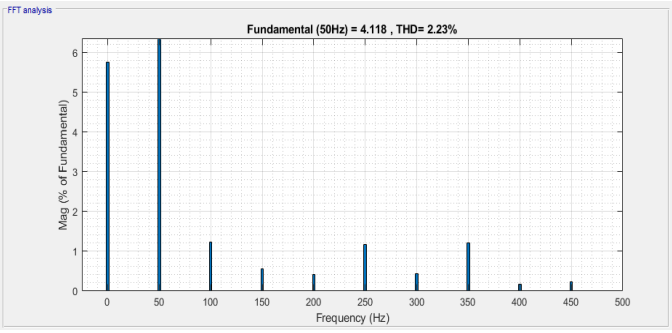

Figure 9: Obtained stator current FFT waveform for a 30º DPWM with torque PI control

FOREX Publication
Open Access | Rapid and quality publishing
International Journal of Electrical and Electronics Research (IJEER)
Research Article | Volume 11, Issue 3 | Pages 652-657 | e-ISSN: 2347-470X

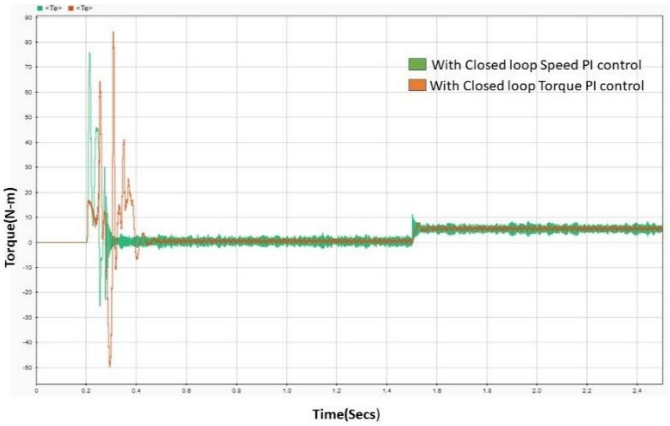

Figure 7: Torque comparison waveform of a 30º DPWM-based closed-loop v/f control with speed PI and torque PI control

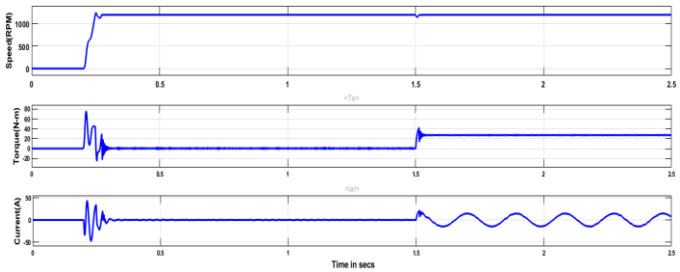

Figure 8: Torque, Current & Speed responses of a 30° DPWM closed-loop constant v/f control with torque PI control

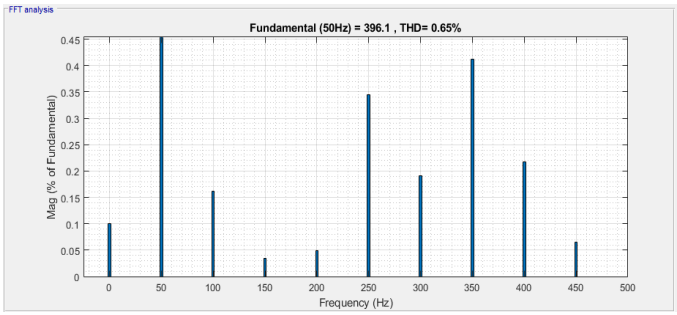

Figure 10: Obtained stator voltage FFT waveform for a 30º DPWM with torque PI control

7. EXPERIMENTAL RESULTS AND DISCUSSIONS

Using the SPARTAN6 FPGA board and a 3-phase inverter, the experiment is carried out for both PI based speed and torque control with 30º DPWM for a 0.75KW induction motor. *Figure 12* snapshot shows the summary of the hardware setup. The implementation was developed in the Xilinx ISE environment and then downloaded to an FPGA board, where the pulses were fed into a 3-phase two-level inverter. The QIP sensor is employed to measure the induction motor's speed.

The torque is estimated from feedback on three phase current parameters. The drive system is initially run in an open loop for a variety of speed commands at rated V/f and no load; *Figure 11b* illustrates the open loop speed, torque, and current responses with inverter's output voltage *figure 11a*. *Figure 11c* and *11d* show the speed and torque responses for PI torque and speed control. Torque PI control based constant v/f control gives extremely better torque responses with lesser torque ripples.

Squirrel- cage Induction motor – 0.75KW (1.6A)
Inverter -3ϕ
Fundamental frequency -50 Hz
Refspeed-1411RPM
Line –to- Line Voltage – 415v
QIP Speed Sensor
FPGA Board - Spartan 6
Switching Frequency -10 KHz

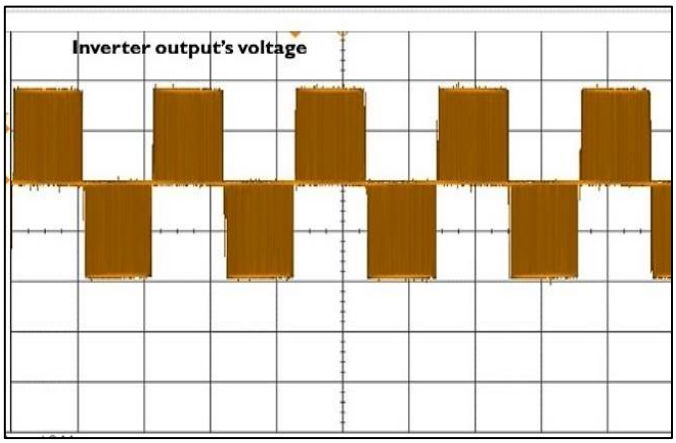

(a)

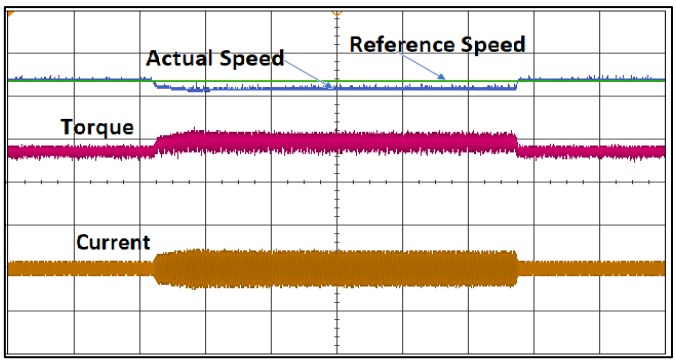

(b)

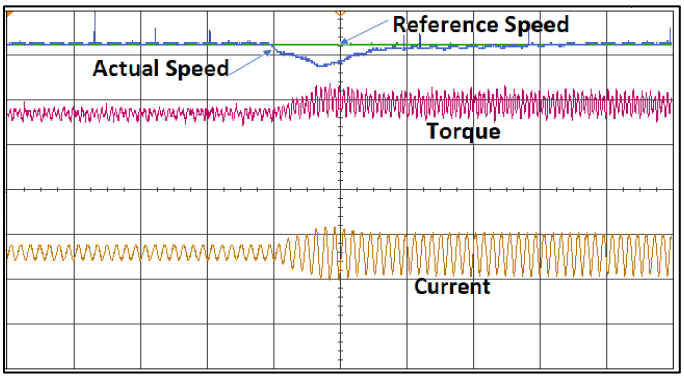

(c)

FOREX Publication
Open Access | Rapid and quality publishing
International Journal of Electrical and Electronics Research (IJEER)
Research Article | Volume 11, Issue 3 | Pages 652-657 | e-ISSN: 2347-470X

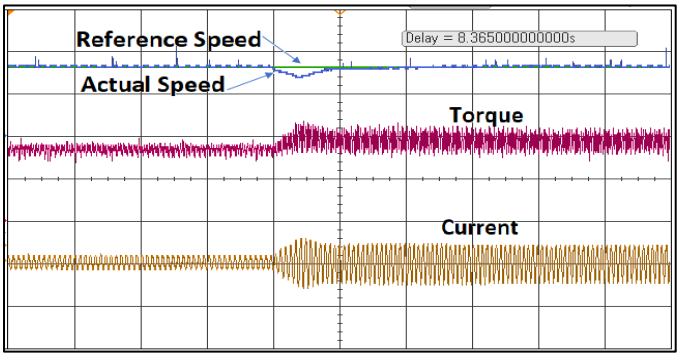

(d)

Figure 11: Observed waveforms at a 50 Hz (fundamental frequency) and 10Khz (Switching frequency) for 30º DPWM with v/f control during the experimentation (a) Two level inverter output voltage (b) Open loop torque and speed responses (c). Torque and speed responses with Torque PI control (d) Torque and speed responses with Speed PI control

Figure 12: Photography of hardware setup

8. APPLICATIONS

Across the nation, electric utility vehicles are becoming more prevalent on farms, pastures, and other terrain. The closed-loop v/f control for the IMD (Induction Motor Drive) makes the suggested speed control approach reliable, simple to use, and ideal for applications requiring minimal precision. Moreover, compared to other vector control techniques, the proposed torque control technique's ease of implementation and affordable cost make it more adaptable to vehicles that do the same task, such as electric mini trucks and quad bikes, in any hilly terrain.

9. CONCLUSION

This paper shows 30º DPWM implementation for new closed-loop v/f control of an induction motor with torque control. The speed PI and torque PI controller based on constant v/f control models have been simulated using the MATLAB/Simulink environment. In comparison to the speed PI based constant v/f control, the analytical, simulation, and experimental findings for the torque PI based constant v/f control represent a better reduction in torque ripple and harmonics in stator current. Torque is estimated with an estimator in a sensor less way, which brings about better control of torque. As a result, the performance objectives of the drive system are well met. For future scope, it is also proposed to try and implement the interval type 2 fuzzy (IT2F) method replacing PI based control, as the IT2F type phenomenally reduces torque ripples to achieve better results, as cited in contemporary articles.

REFERENCES

[1] A. Goedtel, I. N. da Silva, and P. J. A. Serni, “Load torque identification in induction motor using neural networks technique,” Elect. Power Syst. Res., vol. 77, no. 1, pp. 35–45, Jan. 2007.

[2] B. Lu, T. G. Habetler, and R. G. Harley, “A survey of efficiency-estimation methods for in-service induction motors,” IEEE Trans. Ind. Appl., vol. 42, no. 4, pp. 924–933, Jul./Aug. 2006.

[3] D. Shi, P. J. Unsworth, and R. X. Gao, “Sensor less speed measurement of induction motor using Hilbert transform and interpolated fast Fourier transform,” IEEE Trans. Instrum. Meas., vol. 55, no. 1, pp. 290–299, Feb. 2006.

[4] S. Maiti, C. Chakraborty, Y. Hori, and M. C. Ta, “Model reference adaptive controller-based rotor resistance and speed estimation techniques for vector-controlled induction motor drive utilizing reactive power,” IEEE Trans. Ind. Electron., vol. 55, no. 2, pp. 594–601, 2008. 760 IEEE TRANSACTIONS ON INDUSTRIAL ELECTRONICS, VOL. 58, NO. 3, MARCH 2011.

[5] B. Singh, G. Bhuvaneswari, and B. Garg, “Harmonic mitigation in AC–DC converters for vector-controlled induction motor drives,” IEEE Trans. Energy Convers., vol. 22, no. 3, pp. 637–646, Sep. 2007.

[6] B. Karanayil, M. F. Rahman, and C. Grantham, “Online stator and rotor resistance estimation scheme using artificial neural networks for vector-controlled speed sensorless induction motor drive,” IEEE Trans. Ind. Electron., vol. 54, no. 1, pp. 167–176, Feb. 2007.

[7] A. Paladugu and B. H. Chowdhury, “Sensorless control of inverter-fed induction motor drives,” Elect. Power Syst. Res., vol. 77, no. 5/6, pp. 619–629, Apr. 2007.

[8] F. Zidani, D. Diallo, M. E. H. Benbouzid, and R. N. Saïd, “A fuzzy-based approach for the diagnosis of fault modes in a voltage-fed PWM inverter induction motor drive,” IEEE Trans. Ind. Electron., vol. 55, no. 2, pp. 586– 593, Feb. 2008.

[9] M. N. Uddin, Z. R. Huang, and M. I. Chy, “A simplified self-tuned neurofuzzy controller-based speed control of an induction motor drive,” in Proc. IEEE Power Eng. Soc. Gen. Meet., 2007, pp. 1–8.

[10] E. Bim, “Fuzzy optimization for rotor constant identification of an indirect FOC induction motor drive,” IEEE Trans. Ind. Electron., vol. 48, no. 6, pp. 1293–1295, Dec. 2001.

[11] P. P. Cruz and J. P. S. Paredes, “Artificial intelligence applications in direct torque control,” in Proc. 5th Int. Conf. PEDS, 2003, vol. 2, pp. 1208–1212.

[12] Bilal Abdullah Nasir (2022), Performance Improvement of Induction Motor Controlled by Thyristor Chopper on the Rotor Side. IJEER 10(4), 1154-1158. DOI: 10.37391/IJEER.100463.

[13] Karthick Kanagarathinam, R. Manikandan and Ravivarman S (2023), Impact of Stator Slot Shape on Cogging Torque of BLDC Motor. IJEER 11(1), 54-60. DOI: 10.37391/IJEER.110108.

[14] G. El-Saady, A. M. Sharaf, A. Makky, M. K. Sherbiny, and G. Mohamed, “A high performance induction motor drive system using fuzzy logic controller,” in Proc. 7th Mediterranean Electrotech. Conf., 1994, vol. 3, pp. 1058–1061.

[15] R. Krishnan, Electric Motor Drives—Modeling, Analysis, and Control. Upper Saddle River, NJ: Prentice-Hall, 2001.

[16] I. Leon, S. Kouro, L. G. Franquelo, J. Rodriguez, and B. Wu, “The essential role and the continuous evolution of modulation techniques for voltage-source inverters in the past, present, and future power

International Journal of
Electrical and Electronics Research (IJEER)
Research Article | Volume 11, Issue 3 | Pages 652-657 | e-ISSN: 2347-470X

electronics," IEEE Trans. Ind. Electron, Vol. 63, no. 5, pp. 2688–2701, 2016.

[17] Nandhini, E., & Sivaprakasam, A. (2020). A Review of Various Control Strategies Based on Space Vector Pulse Width Modulation for the Voltage Source Inverter. IETE Journal of Research, 1-15.

[18] G. Handley, and J. T. Boys, "Practical real-time PWM modulators: An assessment," IEE Proc. B-Electric Power Appl., Vol. 139, no. 2, IET, 1992.

[19] A. M. Hava, R. J. Kerkman, and T. A. Lipo, "A high performance generalized discontinuous PWM algorithm," IEEE Trans. Ind. Appl., Vol. 34, no. 5, pp. 1059–1071, 1998.

[20] K. Taniguchi, Y. Ogino, and H. Irie, "PWM technique for power MOSFET inverter," IEEE Trans. Power Electron., Vol. 3, no. 3, pp. 328–334, 1988.

[21] A. Sivaprakasam & E. Nandhini (2021): 30° Discontinuous PWM-Based Closed Loop Volts/Hz Control of Induction Motor Drive with Slip Regulation, IETE Journal of Research, DOI: 10.1080/03772063.2021.2004457

[22] Narayanan, G., & Ranganathan, V. T. (2000). Triangle-comparison approach and space vector approach to pulse width modulation in inverter fed drives. Journal of the Indian Institute of Science, 80, 409-427.

[23] Das, S., Hari, V. P. K., Kumar, A., & Narayanan, G. (2019). Analysis of generalized continual-clamp and split-clamp PWM schemes for induction motor drive. Sādhanā, 44(2), 36.

[24] Narayanan, G., Krishnamurthy, H. K., Zhao, D., & Ayyanar, R. (2006). Advanced bus clamping PWM techniques based on space vector approach. IEEE Transactions on Power Electronics, 21(4), 974-984.

[25] Nair, M. D., Biswas, J., Vivek, G., & Barai, M. (2017). Performance Evaluation of Various Bus Clamped Space Vector Pulse Width Modulation Techniques. Journal of Power Electronics, 17(5), 1244-1255.

[26] H. V. D. Broeck, H. C. Skudelny, and G. Stanke, "Analysis and realization of a pulse width modulator based on voltage space vectors," IEEE Trans. Ind. Appl, Vol. 24, no. 1, pp. 142–150, Jan/Feb. 1988. 18.

[27] G. Narayanan, and V. T. Ranganathan, "Synchronised PWM strategies based on space vector approach. Part 1: Principles of waveform generation," Proc. Inst. Elect. Eng., Vol. 146, no. 3, pp. 267–275, May. 1999.

[28] D. Zhao, G. Narayanan, and R. Ayyanar, "Switching loss characteristics of sequences involving active state division in space vector based PWM," Proc. IEEE APEC, Vol. 04, pp. 479–485, Feb. 2004.

[29] Hafeez, M., Uddin, M. N., Rahim, N. A., & Hew, W. P. (2014). Self-tuned NFC and adaptive torque hysteresis-based DTC scheme for IM drive. IEEE Transactions on Industry Applications, 50, 1410–1420.

[30] El Ouanjli, Najib, et al. "Modern improvement techniques of direct torque control for induction motor drives-a review." Protection and Control of Modern Power Systems 4.1 (2019): 1-12.

[31] Arumugam, Sivaprakasam & Manigandan, Thathan. (2014). A Novel Method to Minimize Torque Ripple, Mechanical Vibration, and Noise in a Direct Torque Controlled Permanent Magnet Synchronous Motor Drive. International Journal of Acoustics and Vibrations. 19. 179-189. 10.20855/ijav.2014.19.3351.

[32] Kathiresan, J., & Jothimani (2022), G. High Gain Converter Design and Implementation for Electric Vehicles. International Journal of Electrical and Electronics Research (IJEER), Volume 10, Issue 4, Pages 262-271, e-ISSN: 2347-470X.